CHEMISTRY OF MATERIALS

ARTICLE

pubs.acs.org/cm

Solving the Structure of Li Ion Battery Materials with Precession Electron Diffraction: Application to Li_2CoPO_4F

Joke Hadermann,*[,†] Artem M. Abakumov,[†] Stuart Turner,[†] Zainab Hafideddine,[†] Nellie R. Khasanova,[‡] Evgeny V. Antipov,[‡] and Gustaaf Van Tendeloo[†]

[†]Electron Microscopy for Materials Science (EMAT), University of Antwerp, Groenenborgerlaan 171, Antwerp 2020, Belgium

[‡]Department of Chemistry, Moscow State University, 119991 Moscow, Russia

Supporting Information

ABSTRACT: The crystal structure of the Li_2CoPO_4F high-voltage cathode for Li ion rechargeable batteries has been completely solved from precession electron diffraction (PED) data, including the location of the Li atoms. The crystal structure consists of infinite chains of CoO_4F_2 octahedra sharing common edges and linked into a 3D framework by PO_4 tetrahedra. The chains and phosphate anions together delimit tunnels filled with the Li atoms. This investigation demonstrates that PED can be successfully applied for obtaining structural information on a variety of Li-containing electrode materials even from single micrometer-sized crystallites.

KEYWORDS: lithium, battery material, precession electron diffraction, crystal structure

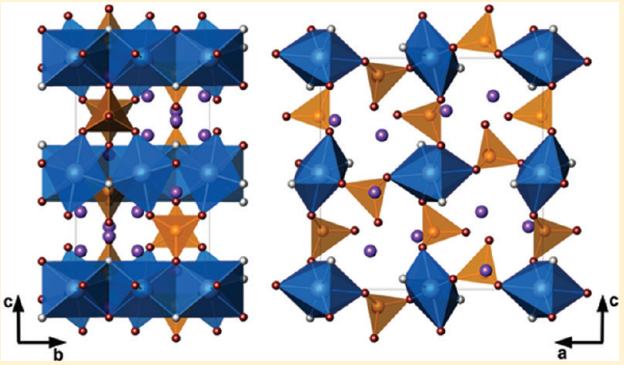

INTRODUCTION

Li-containing transition-metal compounds with polyanions $(XO_n)^{m-}$ (X = P, S, Si, B) in their structures are considered as a promising replacement of conventional oxide cathode materials for lithium ion rechargeable batteries.[1−4] Mixed phosphates, such as $LiFePO_4$, demonstrate a high electrochemical and thermal stability, mainly ascribed to the 3D framework structure, where the metal−oxygen polyhedra are linked to each other by the polyanion units.[2] Further advances in the polyanion Li-based cathodes are related to combining $(XO_n)^{m-}$ and F^- in the anion sublattice.[5−7] It is supposed that the higher electronegativity of fluorine and the higher ionicity of the transition metal to fluorine bonds would allow enhancement of the operating potential, making these materials suitable for a high-voltage cathodes. Li_2CoPO_4F is one promising candidate for high-voltage cathode material working in the 3.0−5.5 V potential range.[8−11] Recent investigation of Li_2CoPO_4F revealed an irreversible structural rearrangement, appearing during cycling between 3 and 5.1 V vs Li^+/Li, with an increase of cell parameters which can enhance lithium conductivity.[9] Therefore, knowledge on the structural behavior of this material at different stages of the charge/discharge cycle can be the key to understanding its performance.

However, even the crystal structure of pristine Li_2CoPO_4F is not known in detail. It crystallizes in an orthorhombic unit cell with *Pnma* space symmetry. Okada et al. suggest a tentative distribution of the atom species over the crystallographic positions of the *Pnma* space group, but do not provide information on the exact location of the Li atoms or on their coordination environment.[8] It was assumed that Li_2CoPO_4F is isostructural to Li_2NiPO_4F on the basis of the similarity of their powder X-ray diffraction patterns.[9,12]

We propose to use precession electron diffraction (PED) for a complete determination of the Li_2CoPO_4F structure. The development of PED has made it feasible to determine atomic coordinates for inorganic compounds from electron diffraction experiments, significantly diminishing the dynamical diffraction effects inherent to electron diffraction.[13−16] In a PED experiment, the electron beam is precessed on a cone with a frequency of ∼100 Hz, with its vertex fixed on the crystallite to be investigated. The recorded pattern is the result of the integration over the different slightly out-of-orientation patterns obtained during the precession movement. In each of these patterns, only a limited amount of reflections, lying along an arc on the Ewald sphere, are excited. This reduces the dynamical effects, making the intensities of the integrated reflections quasi-kinematic and useful for structure solution and refinement.[17] Crystal structures with a combination of heavy and light scatterers (for example, Pb cations and oxygen anions) present essential difficulties for PED because the high scattering density increases the probability of multiple interactions between the electron beam and crystal; hence, the dynamical effects become quite substantial.[18−20] However, modern Li-based battery materials seem to be free of these disadvantages. The requirement of high energy density, low cost, and low toxicity restricts the chemical composition mainly to 3d transition-metal

Received: May 3, 2011
Revised: June 22, 2011
Published: July 11, 2011

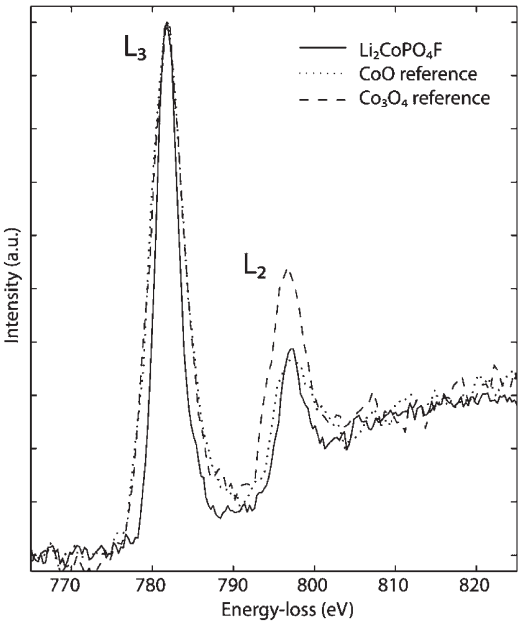

Figure 1. ELNES of the Co $L_{2,3}$ edge of Li_2CoPO_4F. Reference $L_{2,3}$ edges for Co^{2+} (CoO) and $Co^{2.66+}$ (Co_3O_4) are also displayed.

cations and light anions (O^{2-}, F^-, and $(XO_n)^{m-}$ (X = P, S, Si, B)). Thus, one can expect that dynamical scattering will not be a main obstacle for the structure investigation of Li-based cathode materials with PED. A first successful attempt to resolve the structure of a mixed Li and transition-metal oxide with PED was performed on the $Li_4Ti_8Ni_3O_{21}$ compound, where Li and the transition-metal cations jointly occupy the crystallographic positions, with a lowest scattering power approximately twice as high as that for the pure Li cation.[21]

In this paper, we demonstrate that PED can be successfully applied for the solution of the crystal structure of Li-based battery materials. We provide a complete structural characterization of Li_2CoPO_4F, including the location of all Li atoms and the determination of their coordination environment. This achievement opens wide opportunities in understanding the Li intercalation/deintercalation processes in a variety of materials, which are often used in a nanoparticle form in electrochemical experiments, present in polyphasic mixtures or available only in small quantities from electrochemical cells. These circumstances can hamper conventional powder X-ray or neutron diffraction studies, but they are no obstacle for PED since electron diffraction data can be obtained from a single crystallite of the material.

EXPERIMENTAL SECTION

Li_2CoPO_4F has been prepared as described in ref 9. Samples for transmission electron microscopy were made by crushing the powder in ethanol and depositing a drop of this solution on a copper grid covered with a holey carbon film.

PED patterns were obtained with a Philips CM20 equipped with a Spinning Star precession instrument. All PED patterns were obtained using a precession angle of 2.5°. High-angle annular dark field scanning transmission electron microscopy (HAADF-STEM) and high-resolution transmission electron microscopy (HRTEM) images were obtained with an FEI Titan 80-300 "cubed" microscope equipped with image and probe aberration correctors operated at 300 kV. Electron energy loss spectra were acquired on a JEOL 3000F (300 kV) microscope equipped

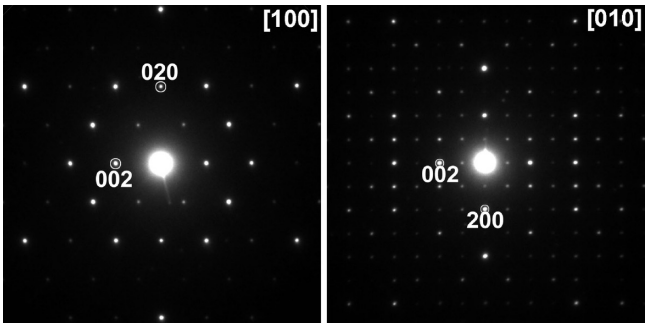

Figure 2. PED patterns of Li_2CoPO_4F.

with a GIF2000 spectrometer. For Li_2CoPO_4F, the microscope was operated in diffraction mode, using a convergence semiangle α of 1 mrad and an acceptance semiangle β of 2 mrad at an energy resolution of ~1 eV. The reference spectra for CoO and Co_3O_4 were acquired in STEM—electron energy loss spectroscopy (EELS) mode using a convergence semiangle α of 10 mrad and an acceptance semiangle β of 28 mrad at an energy resolution of ~1.3 eV. All spectra were background subtracted, aligned to their Co L_3 maximum at 782 eV, and normalized to their maxima.

The PED patterns were treated using the Calidris software (ELD, TRIPLE).[22] Calculated PED patterns and HRTEM images were obtained using JEMS.[23] Structure determination with direct methods was performed using SIR2008,[24] and the refinement of the structure was done using JANA 2006.[25]

RESULTS

The Co oxidation state was verified using EELS by inspecting the energy loss near-edge structure (ELNES) signature of the Co $L_{2,3}$ edge. The ELNES fine structure of the Co $L_{2,3}$ edge at 779 eV has been reported to be a fingerprint for the Co valence state. Indeed, the Co $L_{2,3}$ edge is sensitive to the valence state of cobalt via the so-called white line ratio (WLR), i.e., the ratio between the areas under the L_3 and L_2 edges.[26] The background-subtracted Co $L_{2,3}$ edge for Li_2CoPO_4F is displayed in Figure 1, together with the Co $L_{2,3}$ edge spectra of reference materials CoO (Co^{2+}) and Co_3O_4 ($Co^{2.66+}$). The spectra clearly suggest that Co in Li_2CoPO_4F is in a divalent state, in agreement with the bulk chemical composition.

PED patterns were obtained for 13 different zones ([100], [010], [110], [120], [130], [160], [211], [221], [241], [251], [452], [230], and [041]). The PED patterns along the [100] and [010] zone axes are shown in Figure 2. All PED patterns can be indexed with an orthorhombic unit cell with the cell parameters as refined from X-ray powder diffraction data: a = 10.452(2) Å, b = 6.3911(8) Å, c = 10.874(2) Å.[9] The reflection conditions derived from the PED patterns are hkl (no conditions), $0kl$ ($k + l = 2n$), and $hk0$ ($h = 2n$), consistent with the *Pnma* space group.

The PED patterns were checked for possible overlap of zeroth-order Laue zone reflections with reflections from higher order Laue zones using calculated PED patterns for an angle of 2.5° (JEMS); none of the PED patterns demonstrate such overlap, so the whole range of zeroth-order Laue zone reflections can be used for solution and refinement. Each of the PED patterns produced a separate list of reflections (extraction with ELD). The intensities of the symmetrically equivalent reflections in the 2D data sets were averaged according to the *Pnma* space group (using TRIPLE). The R_{sym} factors that express the agreement of each pattern with the imposed *Pnma* symmetry and the number of unique reflections in each pattern can be found in the Supporting

dx.doi.org/10.1021/cm201257b |*Chem. Mater.* 2011, 23, 3540–3545

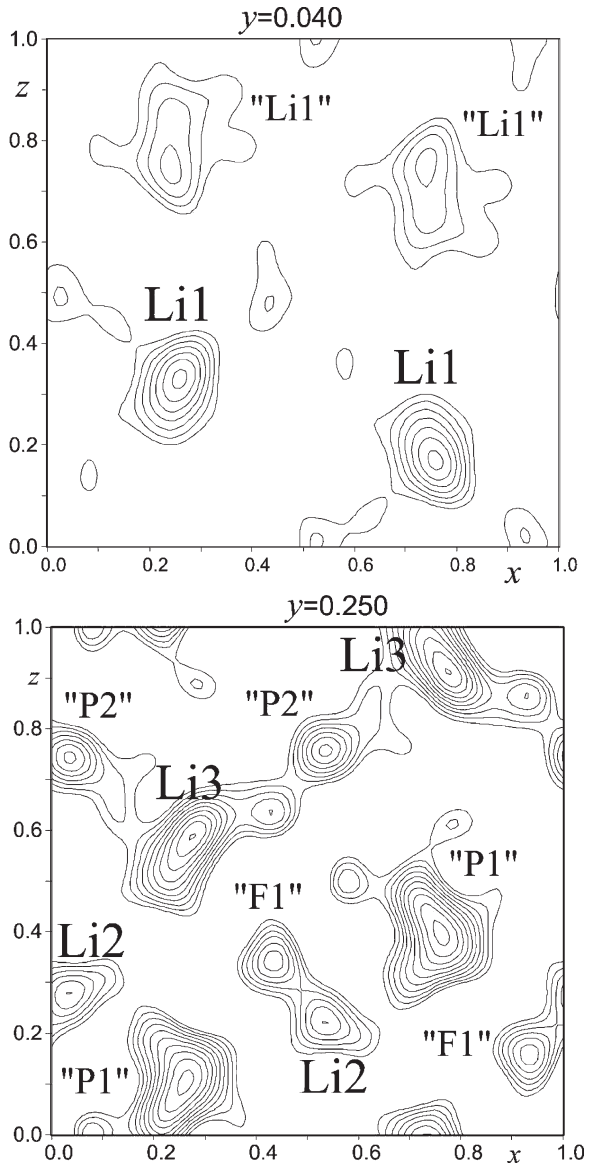

Figure 3. 2D sections of 3D difference Fourier maps with the maxima corresponding to the Li atoms. Spurious maxima from neighboring atoms are labeled in quotes.

Information, Table S1. All intensities were then multiplied with the geometrical correction factor $C(\mathbf{g},R) = \mathbf{g}(1 - (\mathbf{g}/2R)^2)^{1/2}$ ($\mathbf{g}$ is the reciprocal vector, and R is the radius of the Laue circle).[27] Using TRIPLE, the 2D data sets were merged into a 3D data set by using the common reflections between the patterns to calculate scaling factors for each pattern. The order of merging, number of common reflections, and R_{merge} factors expressing the agreement between the relative intensities for the common reflections can be found in Table S2 of the Supporting Information. The intensities of the symmetry-equivalent reflections in the 3D data set were again averaged according to the *Pnma* symmetry. This provided a data set with 237 symmetrically unique reflections, with d values ranging from 7.54 to 0.88 Å, with 100% completeness in the range of $d = 8-5$ Å, 74% completeness for $d = 3-2$ Å, and 41% completeness for $d = 2-1$ Å.

The PED data were used as input for direct methods, together with the cell parameters and the chemical composition. The measured intensities were taken to be proportional to $|F|^2$. A solution was found by direct methods with a final R value of 0.31. In this solution, the Co and P atoms are at positions similar to those in the Li_2NiPO_4F structure.[12] Inspection of the interatomic distances of other maxima on the map with normalized structure factors allows them to be assigned to other atomic species, such as O/F and Li. The atomic coordinates in this solution are given in Table S3 of the Supporting Information. The O/F anions form octahedra around the cobalt atoms and tetrahedra around the P atoms. The remaining peaks can be either Li or ghost atoms; therefore, difference Fourier maps were calculated using the obtained model including Co, P, F, and O only to find the positions of the Li atoms.

Table 1. Selected Crystallographic Parameters for Li_2CoPO_4F

molecular formula	Li_2CoPO_4F
space group	*Pnma*
a, Å	10.452(2)
b, Å	6.3911(8)
c, Å	10.874(2)
Z	8
cell volume, Å^3	726.4
calculated density, g/cm^3	3.415
radiation	electrons, λ = 0.025 Å
no. of reflns	326
no. of params refined	28
R_F	0.24

The difference Fourier maps were calculated using the same diffraction data as used for the direct methods. The positive peaks of the scattering density corresponding to the positions of the Li(1) atoms can be clearly discriminated from the noise and artifacts on the 2D section of the 3D difference Fourier maps (Figure 3). The maxima corresponding to the Li(2) and Li(3) positions are also visible, but less clear due to the presence of residual peaks from heavier atoms in the structure (mostly P and anions). However, calculating the distances from these maxima to other atoms in the model allows us to assign them to the Li atoms undubiously.

For the final refinement of the completed model, the separate 2D sets of structure factors (326 reflections) were used instead of the merged 3D data set. Each 2D set was treated with a separate refineable scale factor. This approach allows us to avoid cumulative errors arising from a subsequent merging of a large number of 2D sets into a single 3D set. The number of reflections used in the refinement is higher than the number of symmetrically independent reflections because the symmetry averaging was performed only within the 2D data sets, but not between the 2D data sets. Due to the relatively low number of reflections, the amount of refineable parameters should be reasonably restricted. Because the phosphate group, PO_4, is a structural unit with a quite rigid geometry, the rigid-body approximation was applied to it. The PO_4 groups were described as perfect tetrahedra with $d(P-O) = 1.53$ Å. Because the phosphorus atoms of the PO_4 groups are located at the m_b mirror planes, the position and orientation of the tetrahedra can be described using only three parameters: the x and z coordinates of the P atom and the rotation angle around the b axis. Thus, the 18 variable atomic coordinates of the two symmetrically independent PO_4 groups are effectively reduced to only 6 parameters. An ordered

Table 2. Positional and Atomic Displacement Parameters for Li_2CoPO_4F

atom	position	x/a	y/b	z/c	U_{iso}, Å^2
Li(1)	8*d*	0.724(13)	0.963(11)	0.665(5)	0.014(2)
Li(2)	4*c*	0.936(14)	3/4	0.729(9)	0.014(2)
Li(3)	4*c*	0.244(19)	1/4	0.581(7)	0.014(2)
Co(1)	4*a*	0	0	0	0.014(2)
Co(2)	4*b*	0	0	1/2	0.014(2)
P(1)	4*c*	0.739(3)	3/4	0.9278(12)	0.014(2)
P(2)	4*c*	0.008(3)	1/4	0.7470(13)	0.014(2)
O(1)	8*d*	0.800(3)	0.945[a]	0.9833(12)	0.014(2)
O(2)	4*c*	0.596(3)	3/4	0.9562(12)	0.014(2)
O(3)	4*c*	0.759(3)	3/4	0.7885(12)	0.014(2)
O(4)	8*d*	−0.041(3)	0.445[a]	0.6808(13)	0.014(2)
O(5)	4*c*	0.154(3)	1/4	0.7466(12)	0.014(2)
O(6)	4*c*	−0.041(3)	1/4	0.8798(13)	0.014(2)
F(1)	4*c*	0.047(6)	3/4	0.877(4)	0.014(2)
F(2)	4*c*	0.872(5)	3/4	0.545(5)	0.014(2)

[a] The coordinate is fixed by the rigid-body geometry.

Table 3. Selected Interatomic Distances for Li_2CoPO_4F

Li(1)−O(1)	2.08(6) × 1	Co(1)−O(1)	2.12(3) × 2
Li(1)−O(3)	1.95(6) × 1	Co(1)−O(6)	2.108(10) × 2
Li(1)−O(4)	2.52(13) × 1	Co(1)−F(1)	2.14(3) × 2
Li(1)−O(5)	2.20(7) × 1	BVS = 1.81(4)	
Li(1)−F(1)	2.35(12) × 1		
Li(1)−F(2)	2.44(10) × 1	Co(2)−O(2)	1.944(14) × 2
BVS = 0.78(7)		Co(2)−O(4)	2.043(14) × 2
		Co(2)−F(2)	2.14(3) × 2
Li(2)−O(2)	2.61(12) × 1	BVS = 2.31(5)	
Li(2)−O(3)	1.97(14) × 1		
Li(2)−O(4)	2.03(3) × 2	P(1)−O(1)	1.53 × 2
Li(2)−F(1)	1.99(12) × 1	P(1)−O(2)	1.53 × 1
Li(2)−F(2)	2.11(11) × 1	P(1)−O(3)	1.53 × 1
BVS = 1.06(13)			
		P(2)−O(4)	1.53 × 2
Li(3)−O(1)	2.15(6) × 2	P(2)−O(5)	1.53 × 1
Li(3)−O(5)	2.03(12) × 1	P(2)−O(6)	1.53 × 1
Li(3)−O(6)	2.29(19) × 1		
Li(3)−F(2)	1.83(15) × 1		
BVS = 0.92(15)			

arrangement of the O and F atoms was assumed taking into account that the F atoms cannot mix with the O atoms of the rigid PO_4 units. The refinement was performed with an overall atomic displacement parameter. The resulting reliability factor was R = 0.24, which is reasonable for pseudokinematical electron diffraction data. The crystallographic parameters, atomic coordinates, and main interatomic distances are listed in Tables 1−3, respectively.

The structure solution was supported by direct space TEM observations. It should be noted that Li_2CoPO_4F is very sensitive to the electron beam in both the TEM and STEM modes at 300 kV as well as at 80 kV acceleration voltage. This prevents any continuous observations, which, for example, would be required for acquiring a through-focus series of HRTEM images for exit

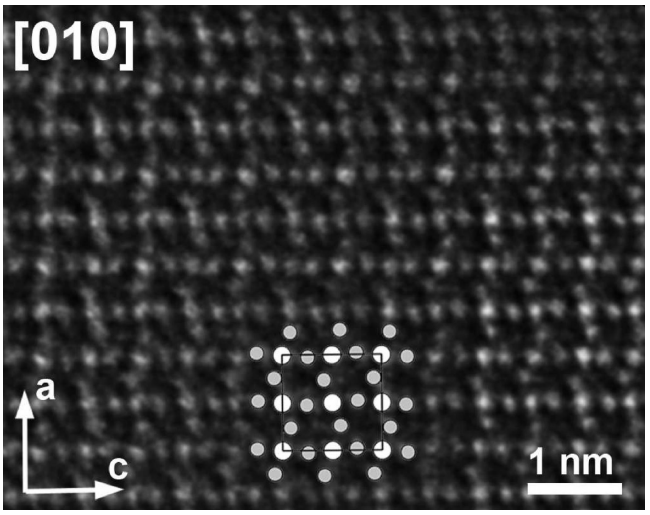

Figure 4. [010] HAADF-STEM image of Li_2CoPO_4F. The structure projection is overlaid with marked positions of the Co columns (large white circles) and P columns (small gray circles).

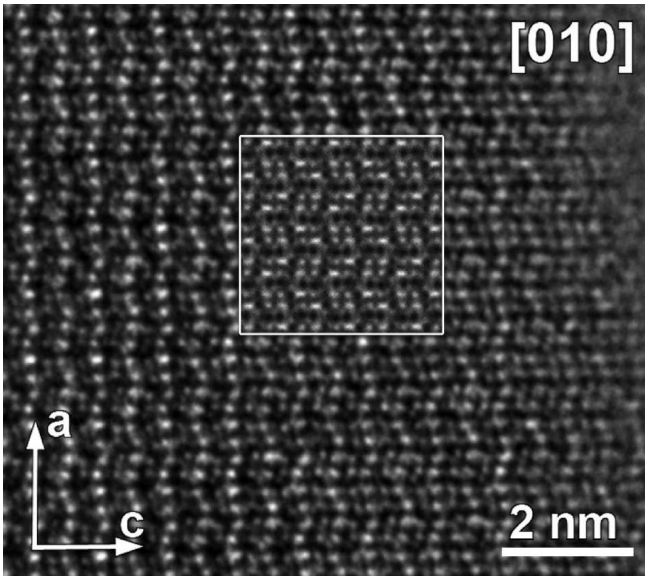

Figure 5. [010] HRTEM image of Li_2CoPO_4F. The calculated image (f = −51 nm, t = 2.6 nm) is shown as an inset (to be compared with the experimental contrast on the right side of the picture).

wave reconstruction. Acquiring HAADF-STEM images can be performed only with a short acquisition time, which results in noisy images requiring subsequent Fourier filtering. Nevertheless, the high-pass-filtered [010] HAADF-STEM image in Figure4 of Li_2CoPO_4F clearly demonstrates the positions of the Co and P atomic columns. The brighter dots correspond to the projection of the Co columns (Z = 27). Each brighter dot is surrounded by four less bright dots forming an elongated rectangle, which corresponds to the positions of the P columns (Z = 15). The arrangement of these dots on the [010] HAADF-STEM image perfectly reproduces the positions of the Co and P atomic columns in the refined structure along this projection. The contrast on the [010] HRTEM image is formed by

dx.doi.org/10.1021/cm201257b |*Chem. Mater.* 2011, 23, 3540–3545

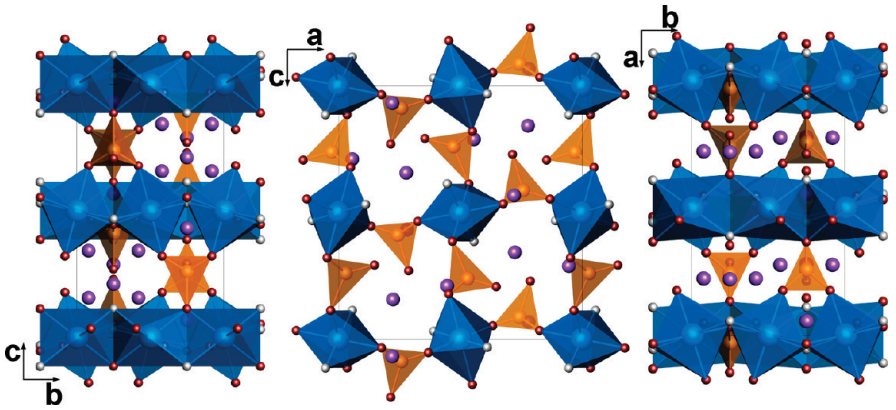

Figure 6. Crystal structure of Li_2CoPO_4F in three different projections. The CoO_4F_2 octahedra are blue, and the PO_4 tetrahedra are orange. The O, F, and Li atoms are shown as small brown, small gray, and larger violet spheres, respectively.

parallelograms of the brighter dots arranged into layers along the *c* axis and having a staggered arrangement along the *a* axis (visible at the thinnest area of the crystallite at the right side of Figure 5). The simulated HRTEM image (focus $f = -51$ nm, thickness $t = 2.6$ nm) is in good agreement with the experimental one. Under these imaging conditions, the brighter dots correspond to low projected potentials (tunnels) in the structure. Each parallelogram of four bright dots is centered with a column of Co atoms.

DISCUSSION

The crystal structure of Li_2CoPO_4F is shown in Figure 6. The crystal structure consists of infinite chains of the CoO_4F_2 octahedra sharing common edges. The chains run along the *b* axis and are linked into a 3D framework by PO_4 tetrahedra. The chains and polyanions together delimit tunnels along the *b* axis, where the Li atoms are located. This structural organization is similar to that of Li_2NiPO_4F[13] and $Li_{1.75}Ni_{0.75}Fe_{0.25}PO_4F$.[10] The CoO_4F_2 octahedra are slightly distorted with nearly equal Co−O and Co−F interatomic distances. The Li atoms are located at irregular 5- and 6-fold-coordinated polyhedra. The bond valence sum (BVS) for the Li(2) and Li(3) cations is equal to the nominal valence +1 in the range of the standard deviation. The BVS for the Li(1) cation (8*d* position) is noticeably lower, indicating that this cation is underbonded in the structure. This suggests that the Li(1) position is responsible for the Li extraction upon chemical or electrochemical oxidation of Li_2CoPO_4F. This conclusion is corroborated by the fact that, upon chemical delithiation of the isostructural $Li_2Ni_{0.75}Fe_{0.25}PO_4F$ compound to the $Li_{1.75}Ni_{0.75}Fe_{0.25}PO_4F$ composition, only the occupancy of the Li(1) position was found to decrease to ~0.75, whereas the occupancies of the Li(2) and Li(3) positions do not noticeably change.[9]

The complete solution of the Li_2CoPO_4F structure demonstrates that PED can be successfully applied for the crystallographic characterization of Li-based battery materials. In fact, the target functional properties (high energy density, high electrochemical stability, high mobility of Li) make the Li-containing transition-metal polyanion structures optimal objects for investigation with PED: the high energy density requires the absence of heavy metal cations. This results in a combination of elements with relatively small atomic numbers, reducing the dynamical electron scattering. The increasing electrochemical stability is related to the presence of polyanions, which are rigid structural units with a well-defined geometry. This allows using the rigid body approximation, resulting in a drastic decrease of the number of structural variables. This is important because of the limited amount of diffraction data obtained by PED. The high mobility of Li in such materials is responsible for the instability under an intense electron beam. Decreasing the energy of the incident electron beam does not improve the stability of such materials. The displacement scattering cross section for Li reaches its maximum at nearly 60 kV, making the damage at low accelerating voltage even more severe than at 200−300 kV conventionally used for TEM imaging.[28] In contrast to the direct space imaging techniques, a PED investigation requires parallel illumination with a spread electron beam, keeping the overall irradiation dose at a minimum and leaving the material intact.

PED data can be collected from very small crystals tens or hundreds of nanometers in size and detect various superstructures (even rather weak) appearing at different stages of Li deintercalation processes from electrode materials. Such fine structure changes are not always evident from in situ X-ray diffraction experiments.

The preliminary electron diffraction investigation of chemically delithiated Li_2CoPO_4F revealed formation of a weak superstructure, which can be attributed to ordering of the Li atoms and vacancies. The detailed analysis of the crystal structure of the chemically delithiated phase is now in progress.

ASSOCIATED CONTENT

Supporting Information. Tables with details on the PED patterns used and unrefined atomic coordinates as obtained straight from direct methods (PDF) and CIF file. This material is available free of charge via the Internet at http://pubs.acs.org.

AUTHOR INFORMATION

Corresponding Author

*Phone: +32 3265 3245. Fax: +32 3265 3257. E-mail: joke.hadermann@ua.ac.be.

ACKNOWLEDGMENT

This work was supported by the Research Foundation—Flanders (FWO Grants G.0184.09N and 1.5.005.08), BOF—

University of Antwerp (Grant 23047), and Russian Foundation for Basic Research (RFBR Grant 10-03-00970-a).

REFERENCES

(1) Yamada, A.; Chung, S. C.; Hinokuma, K. *J. Electrochem. Soc.* **2001**, *148*, A224.
(2) Padhi, A. K.; Manivannan, V.; Goodenough, J. B. *J. Electrochem. Soc.* **1998**, *145*, 1518.
(3) Nyten, A.; Abouirmrane, A.; Armand, M.; Gustafsson, T.; Tomas, J. O. *Electrochem. Commun.* **2005**, *7*, 156.
(4) Yamada, A.; Iwane, N.; Harada, Y.; Nishimura, S.; Koyama, Y.; Tanaka, I. *Adv. Mater.* **2010**, *22*, 3583.
(5) Baker, J.; Saidi, M. Y.; Gover, R. K. B.; Burns, P.; Bryan, A. *J. Power Sources* **2007**, *174*, 927.
(6) Ellis, B. L.; Makahonouk, W. R. M.; Makimura, Y.; Toghill, K.; Nazar, L. F. *Nat. Mater.* **2007**, *6*, 749.
(7) Recham, N.; Chotard, J.-N.; Dupont, L.; Delacourt, C.; Walker, W.; Armand, M.; Tarascon, J.-M. *Nat. Mater.* **2010**, *9*, 68.
(8) Okada, S.; Ueno, M.; Uebou, Y.; Yamaki, J. *J. Power Sources* **2005**, *146*, 565.
(9) Khasanova, N. R.; Gavrilov, A. N.; Antipov, E. V.; Bramnik, K. G.; Hibst, H. *J. Power Sources* **2011**, *196*, 355.
(10) Wang, D.; Xiao, J.; Xu, W.; Nie, Z.; Wang, C.; Graff, G.; Zhang, J.-G. *J. Power Sources* **2011**, *196*, 2241.
(11) Dumont-Botto, E.; Bourbon, C.; Patoux, S.; Rozier, P.; Dolleb, M. *J. Power Sources* **2011**, *196*, 2274.
(12) Dutreilh, M.; Chevalier, C.; El-Ghozzi, M.; Avignant, D. *J. Solid State Chem.* **1999**, *142*, 1.
(13) Gemmi, M.; Zou, X.; Hovmuller, S.; Migliori, A.; Vennstrom, M.; Andesson, Y. *Acta Crystallogr.* **2003**, *A59*, 117.
(14) Gjønnes, J.; Hansen, W.; Berg, B. F.; Runde, P.; Cheng, Y. F.; Gjønnes, K.; Dorset, D. L.; Gilmore, C. J. *Acta Crystallogr.* **1998**, *A54*, 306.
(15) Own, C. S.; Sinkler, W.; Marks, L. D. *Ultramicroscopy* **2006**, *106*, 114.
(16) Kverneland, A.; Hansen, V.; Vincent, R.; Gjønnes, K.; Gjønnes, J. *Ultramicroscopy* **2006**, *106*, 492.
(17) Vincent, R.; Midgley, P. A. *Ultramicroscopy* **1994**, *53*, 271.
(18) Weirich, T.; Portillo, J.; Cox, G.; Hibst, H.; Nicolopoulos, S. *Ultramicroscopy* **2006**, *106*, 164.
(19) Boulahya, K.; Ruiz-Gonzàlez, L.; Parras, M.; Gonzàlez-Calbet, J. M.; Nickolsky, M. S.; Nicolopoulos, S. *Ultramicroscopy* **2007**, *107*, 445.
(20) Hadermann, J.; Abakumov, A. M.; Tsirlin, A. A.; Filonenko, V. P.; Gonnissen, J.; Tan, H.; Verbeeck, J.; Gemmi, M.; Antipov, E. V.; Rosner, H. *Ultramicroscopy* **2010**, *110*, 881.
(21) Gemmi, M.; Klein, H.; Rageau, A.; Strobel, P.; Le Cras, F. *Acta Crystallogr.* **2010**, *B66*, 60.
(22) Zou, X. D.; Sukharev, Y; Hovmöller, S *Ultramicroscopy* **1993**, *52*, 436.
(23) Stadelmann, P. A. *Ultramicroscopy* **1987**, *21*, 131.
(24) Burla, M. C.; Camalli, M.; Carrozzini, B.; Cascarano, G. L.; Giacovazzo, C.; Polidori, G.; Spagna, R. *J. Appl. Crystallogr.* **2003**, *36*, 1103.
(25) Petricek, V.; Dusek, M. *JANA2000: Programs for Modulated and Composite Crystals*; Institute of Physics: Praha, Czech Republic, 2000.
(26) Wang, Z. L.; Yin, J. S.; Jiang, Y. D. *Micron* **2000**, *31*, 571.
(27) Gemmi, M.; Nicolopoulos, S. *Ultramicroscopy* **2007**, *107*, 483.
(28) Rossell, M. D.; Erni, R.; Asta, M.; Radmilovic, V.; Dahmen, U. *Phys. Rev. B* **2009**, *80*, 024110.